Testing random forest classification for identification and aging of lava flows from a single Landsat 8 image

Long LI [1, 2], Carmen SOLANA [3], Frank CANTERS [4], Longqian CHEN [1], Matthieu KERVYN [2]

1. School of Environmental Science and Spatial Informatics, China University of Mining and Technology, Daxue Road 1, Xuzhou 221116, China (corresponding author: long.li@vub.be)
2. Department of Geography, Earth System Science, Vrije Universiteit Brussel, Pleinlaan 2, Brussels 1050, Belgium
3. School of Earth and Environmental Sciences, University of Portsmouth, Burnaby Building, Burnaby Road, Portsmouth PO1 3QL, UK
4. Cartography and GIS Research Group, Department of Geography, Vrije Universiteit Brussel, Pleinlaan 2, Brussels 1050, Belgium

Abstract

Mapping lava flows using satellite images is an important application of remote sensing in volcanology. Several volcanoes have been mapped through remote sensing using a wide range of data, from optical to thermal infrared and radar images, using techniques such as manual mapping, supervised/unsupervised classification, and elevation subtraction. So far, spectral-based mapping applications mainly focus on the use of traditional pixel-based classifiers, without much investigation into the added value of object-based approaches and into advantages of using machine learning algorithms. In this study, Nyamuragira, characterized by a series of more than 20 overlapping lava flows erupted over the last century, was used as a case study. The random forest classifier was tested to map lava flows based on pixels and objects. Image classification was conducted for the 20 individual flows and for 8 groups of flows of similar age using Landsat 8 imagery and a DEM of the volcano, both at 30-meter spatial resolution. Results show that object-based classification produces maps with continuous and homogeneous lava surfaces, in agreement with the physical characteristics of lava flows, while lava flows mapped through the pixel-based classification are heterogeneous and fragmented including much “salt and pepper

noise". In terms of accuracy, both pixel-based and object-based classification performs well but the former results in higher accuracies than the latter except for mapping lava flow age groups without using topographic features. It is concluded that despite spectral similarity, lava flows of contrasting age can be well discriminated and mapped by means of image classification. The classification approach demonstrated in this study only requires easily accessible image data and can be applied to other volcanoes as well if there is sufficient information to calibrate the mapping.

Keywords: Lava flows; Nyamuragira; Pixel-based classification; Object-based classification; Random forest;

1 Introduction

Lava flows, the dominant product of effusive eruptions, pose an important threat to the inhabitants on the flanks of active volcanoes and can also reshape landscapes and ecosystems at regional scale. Mapping lava flows enables the estimation of preferred vent locations, area covered by flows and even their volumes. It can also contribute to constrain the return period of effusive events, which is critical for lava flow hazard assessment and management (Kauahikaua and Tilling, 2014). Lava flow mapping is an important application of remote sensing in volcanology. In this study, it is defined exclusively as the delineation of lava flow boundaries and the separation of flow units emitted by different eruptions at different times, although volume estimation is occasionally included in its broader definition (Head et al., 2013; Lu et al., 2004; Smets et al., 2010). Field mapping is frequently obstructed by difficulties in accessibility, the scale of lava flow fields, logistics, topography, climate and politics and remote sensing has become increasingly important in mapping volcanic terrains and specifically in mapping lava flows. Mapping individual lava flows using satellite remote sensing is challenging for at least three reasons: vegetation cover, spatial overlapping and spectral similarity. In a tropical environment with high precipitation and insolation, vegetation grows remarkably fast and can partially or fully cover lava surfaces only a few decades after eruptions (Li et al., 2015a), thus disabling the discrimination of lava flows from the surrounding vegetation on satellite imagery. Moreover, a high eruption frequency often leads to lava flows overlapping each other. If the overlapping lava flows are erupted within a short time span and have similar chemical and surface characteristics, discrimination will be further complicated by their similar spectral signatures. The problems listed might be partially overcome by using better remote sensing data (e.g. with higher spatial (Mazzarini et al., 2007) and/or spectral resolutions), by applying more performant classifiers (e.g. machine learning algorithms) or by switching the classification unit from pixel to object.

Satellite remote sensors allowing lava flow mapping have diversified over the years as a result of advances in remote sensing. An inventory of potentially useful remotely sensed data and their capabilities for mapping volcanic terrains has previously been compiled (Kervyn et al., 2007). For the specific purpose of mapping lava flows, many studies have used optical imagery only (Head et al., 2013; Servadio et al., 2012) because this type of imagery is often easily accessible,

mostly free of charge, yet cloud/snow cover greatly reduces its utility for volcanoes located in tropical regions and/or at high elevations. The capabilities of operating at all times and of penetrating through clouds have nevertheless made radar satellite data achieve a growing prominence in the observation of volcanoes. Radar imagery has been used as single data source in some studies (Favalli et al., 2009; Mahmood and Giugni, 2001; Zebker et al., 1996) but more often in combination with optical imagery for better discrimination due to additional spectral information (Lu et al., 2004; Rowland, 1996; Smets et al., 2010). Use of thermal infrared data has also been examined because the difference in emissivity of lava flows allows them to be discriminated from each another (Abrams et al., 1996, 1991).

Manual mapping through visual interpretation is a practical approach to obtain the extent of a lava flow on remotely sensed data (Smets et al., 2010). It might be time-consuming, particularly when used as the only means of mapping, however it is relatively easy. The resulting lava flow boundaries are usually quite accurate when combining visual interpretation of remotely sensed data with readily available geological maps and field work. Usually being in vector format, the result of the mapping can be directly imported into a geographical information system (GIS) for spatial analysis and for a geological map update.

In addition to the manual mapping approach, pixel-based classification is also an often used technique for volcanic mapping. Nine Etna lava flows erupted in different centuries were mapped through pixel-based classification to revise previously published geological maps (Abrams et al., 1991). An unsupervised classification (ISODATA) was applied on Nyamuragira for mapping 19 lava flows from multiple multispectral satellite images after supervised classification failed (Head et al., 2013). Another unsupervised method (K-Means) was used to identify lava flows of Sabancaya (Peru) with SPOT multispectral and panchromatic imagery (Legeley-Padovani et al., 1997). Classification of Hyperion imagery based on spectral angle mapping was performed for the Holocene Lava Field in Iceland (Aufaristama et al., 2016). All these types of classifiers are commonly used in lava flow mapping applications but no attempts have been made so far to test more advanced classification approaches for mapping lava flows, such as machine learning algorithms (e.g. support vector machines, decision trees, random forest).

Pixel-based classification of lava flows is based on spectral differences between lava flows and their surroundings, such as vegetation and urban infrastructure, and between lava surfaces of various age. In many cases, low spatial resolution imagery contains a large number of mixed pixels which may result in inaccurate classification (Li et al., 2015a). Pixels constituting a mixture of lava flow and vegetation or a mixture of other lava flows of different age are indeed more likely to be misclassified. In addition, spectral heterogeneity exists among pixels that are part of single lava flows: the local environment will control the weathering and vegetation evolution of a lava surface which may differ along a single lava flow (Li et al., 2015a, 2015b). Thanks to the homogenous mixing, these challenges might be solved by using the geographical object-based image analysis (GEOBIA) approach (Blaschke et al., 2014). Object-based classification has been applied for mapping volcanic deposits from SPOT imagery in recent studies focusing on lahars (Kassouk et al., 2014; Thouret et al., 2015), yet the potential of GEOBIA for automated mapping of lava flow fields has so far not been specifically investigated.

In the case of Nyamuragira (DRC), the volcanological map produced by Belgian scientists (Thonnard and Denaeyer, 1965) is probably the first one that delineates lava flows erupted until 1958 based on aerial photographs–with associated errors due to available techniques at the time. The 1990s civil wars in this politically volatile African country have prevented field-based observations and aerial photography acquisition for updating maps with recently emplaced lava flows. Consequently, access to information on Nyamuragira has long relied largely on remote sensing. Since then lava flows have been occasionally mapped, e.g. the 1996 flow from JERS-1 InSAR (Kitagawa et al., 2007) and the 1998 and 2001 flows from ERS InSAR (Colclough, 2006). Recent studies (Head et al., 2013; Smets et al., 2010) have resulted in more comprehensive lava flow maps from multi-temporal satellite imagery, optical or radar. The advantage of the multi-temporal approach is that each lava flow can be accurately mapped from imagery before it becomes vegetated. Discriminating multiple lava flows from a single image, particularly flows overlapping each other, is more challenging but is very interesting, as for some volcanoes good optical satellite data are scarce due to the high frequency of cloud cover. Li et al. (2015a) used spectral mixture analysis to highlight the change in spectral properties and vegetation fraction of lava flows of different age at Nyamuragira. But that study did not investigate whether these contrasting spectral characteristics could be used for automatic mapping of lava flows of different age.

This study aims at proposing strategy for mapping lava flows of tropical volcanoes from a single image by comparing pixel-based versus object-based mapping approaches, using a machine learning based framework for classification (random forest), and consequently at producing a map distinguishing lava flows of different age for Nyamuragira. Depending on the classification unit (pixel or object), the features used and the classification target (individual or grouped lava flows), different classification scenarios are compared in terms of mapping accuracies obtained.

2 Study area

Nyamuragira (aka Nyamulagira) is an active shield volcano in the Virunga National Park in the east of the Democratic Republic of the Congo (DRC). It is situated about 13 km northwest of Nyiragongo volcano and about 25 km north of Lake Kivu (Figure 1). Its summit caldera has a maximum diameter of ~2.3 km (NW-SE) and a maximum depth of ~200 m, partially collapsing in 1938 and draining a previous lava lake (Smets et al., 2010). Characterized by a maximum elevation of 3058 m a.s.l, this volcano has gently rising flanks which host a large number of cones and fissures.

A high frequency of volcanic eruptions, once every 2-4 years, from vents located on or along the flanks, has earned it a reputation as the most active volcano in Africa (Smets et al., 2015, 2010). A total of 27 lava flows erupted from 1938 to 2011 have been currently dated and mapped (Albino et al., 2015; Head et al., 2013; Smets et al., 2010). Most of these lava flows are located on the flanks except for the 1956 flow constrained within the caldera. The 1958 flow advanced farthest to the northeast while the 1938-40 and 1948 flows reached farthest southwest, ending in Lake Kivu.

The recent lava flows are emplaced within the densely forested Virunga National Park. Vegetation recovery after lava emplacement has largely benefited from the equatorial climate. This has a dual effect on image classification: it creates a remarkable contrast between fresh lava surfaces and dense forests but also makes that lava flows become increasingly obscured over time, which is clearly the case for the old ones.

3 Data and methods

3.1 Satellite image data

A Landsat 8 Level-1 image of the study area, acquired on February 9, 2015, was used for lava flow spectral classification in this study (Figure 1). Although the presence of gas and clouds affects part of the image, this scene is the best one that could be obtained following the Landsat ETM+ image acquired on January 31, 2003 (Li et al., 2015a). Digital numbers of the image were converted to radiance values by radiometric calibration and NDVI was then calculated. Atmospheric effect was not corrected for in the study—because atmospheric disturbance is assumed to be homogenous over the area to be classified in the cloud-free part of the image.

Given that the focus of this study is on discriminating different lava flow surfaces, non-lava surfaces should be excluded from the analysis as much as possible. The extent of the lava flow field and the directly adjacent forest was therefore outlined on the image through visual interpretation (Figure 1). As such, ash-, gas- and cloud-affected areas, bare-soil and built-up areas, and more importantly, most of the vegetated areas of the volcanic region, are not taken into account in the classification process. The delineated surfaces include 20 lava flows erupted over the last 70 years excluding the 1938-40 (covered by gas and also fully vegetated), 1951-52 (too small), 1954 (too vegetated), 1956 (too small and also located within the caldera), 1957 and 1986-87 flows (too small on the image because of overlap).

Additionally, thermal information of the Landsat 8 imagery (TIRS) and 30-meter SRTM DEM were also included as ancillary data in support of the image classification process. Brightness temperature was derived from one of the two thermal bands (b11) for the volcanic region following the method in Blackett (2014), as it might help discriminating between young lava and old lava. Elevation and other DEM-derived topographic variables were found to impact vegetation recovery on lava flows and hence topography was also included in the classification.

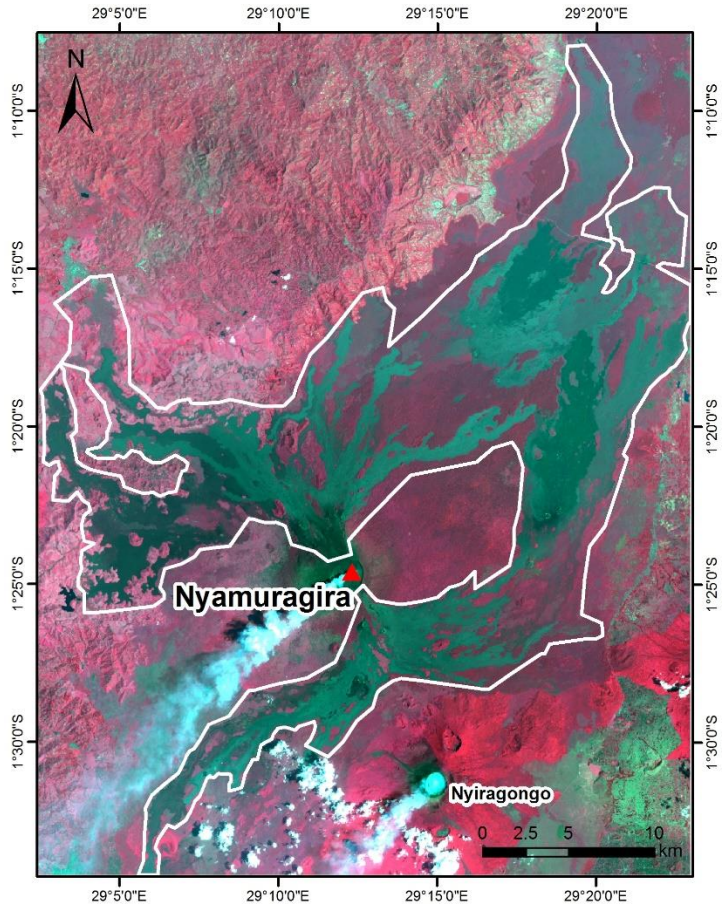

Figure 1 Landsat 8 image (Feb-9-2015) of Nyamuragira's lava flows, showing the manually outlined area used for segmentation and classification.

3.2 Random forest

In this study, all the image classification was conducted using random forest (RF). Random forest is a popular and efficient machine learning approach used for both classification and regression purposes. It has been used in a wide range of applications including remote sensing image classification with improved accuracies (Eisavi et al., 2015; Gislason et al., 2006). A review of random forest in remote sensing has been published recently (Belgiu and Drăguț, 2016). A random forest classifier grows an ensemble of binary decision trees by selecting a fraction of bootstrap samples out of input data and choosing randomly a subset of explanatory variables for each split (Breiman, 2001; Genuer et al., 2010). Each decision tree, which is unpruned (i.e. no restriction is imposed to control its depth), returns a classification and random forest decides to which class each observation is attributed based on applying a majority rule: the

class that has the most votes across all trees is determined as the final class (Breiman, 2001). The input data selected for training each of the trees are in-bag observations and the remaining are out-of-bag (OOB) observations used for estimating OOB errors (misclassifications). When the values of a feature (i.e. an explanatory variable) are randomly permuted, the increase in the mean OOB error is defined as the feature importance (Boulesteix et al., 2012; Genuer et al., 2010). It is noted that feature rankings can be misleading when there are high correlations between the features (correlation coefficient r >0.8 in this study) (Gregorutti et al., 2016; Strobl et al., 2008; Tolosi and Lengauer, 2011). A simple strategy was therefore applied in this study to decorrelate the features by excluding one of any of two highly correlated features.

There are three parameters to be tuned when applying random forest classification: the fraction of observations used for training, the number of decision trees (*ntree*) and the number of features randomly selected at each node (*mtry*). Random forest is usually not very sensitive to their values (Liaw and Wiener, 2002). By default, random forest takes roughly two thirds of the samples with replacement for growing decision trees and the OOB errors are estimated based on the remaining one third. In general, with an increase in the number of grown trees, the OOB error decreases and eventually levels off so a larger value of *ntree* does not always yield more reliable results than a smaller one. The default and optimal value for *mtry* is $\sqrt{p}$ for classification, where p is the number of available features (Breiman, 2001). The default *mtry* is optimal with respect to prediction accuracy but it is recommended to consider different values in the case of highly correlated features (Strobl et al., 2008). In this study, different values for *ntree* and *mtry* are tested and the pair that yields the lowest OOB error will be considered optimal. The candidate values for *ntree* are from 500 to 5000 with increments of 500, which have been frequently used in previous studies (Eisavi et al., 2015; Genuer et al., 2010; Gislason et al., 2006). Numbers higher than 5000 were not tested because they are computationally expensive and usually do not yield more reliable results than smaller values (Boulesteix et al., 2012). Regarding *mtry*, it is recommend by Prof. Breiman, who developed random forest, to pick the best one from the default value, half of the default value and twice the default value (Liaw and Wiener, 2002).

In this study, use was made of the random forest implementation available in Matlab. Both pixel-based and object-based classification was conducted using the random forest classifier and compared in terms of classification accuracy.

3.3 Pixel-based classification

For pixel-based random forest classification, candidate features include the radiance of the first seven multispectral bands (b1-b7), NDVI, brightness temperature (BT) from band 11 and topographic features. Among them, b2 (Blue) is highly correlated with b1 (Coastal aerosol; CA) (r >0.98) and with b4 (Red) (r >0.86), and b5 (NIR) is highly correlated with NDVI (r >0.93). As a result, both b2 and b5 were excluded from classification. Topographic features, including elevation, slope and aspect (categorical feature derived from the DEM resampled at 1 km) were considered as optional (Table 1). In order to assess the usefulness of topographic data, pixel-based classification was performed with 10 features including topography and with 7 features excluding topography. For the pixel-based classification, a total of 2050 individual pixels were manually sampled on the Landsat 8 image for vegetation and lava flows, with about 100 pixels for vegetation and lava flows of contrasting age.

Table 1 Input features for pixel-based random forest classification

Landsat 8 data	b1 (CA), b3 (Green), b4 (Red), b6 (SWIR1), b7 (SWIR2), NDVI
	BT (brightness temperature)
Topographic data	Elevation, Slope, Aspect (Categorical)

3.4 Image segmentation

Satellite images show relatively sharp edges between different lava flows and between lava flows and vegetated areas, which might enable the use of geographical object-based image analysis (GEOBIA). In addition to spectral characteristics, this approach can also take spatial, textural and contextual information into account. It has been extensively reported to outperform both pixel-based supervised and unsupervised classification in different contexts (Blaschke, 2010; Demarchi et al., 2016; Myint et al., 2011; Riggan and Weih, 2009; Weih and Riggan, 2010).

The first step of GEOBIA is image segmentation, where the image is segmented into objects of different sizes, which will then be used as classification units. Image segmentation in the study was performed in eCognition. Data used for image segmentation consisted of the multispectral bands (b1 to b7) of the Landsat 8 OLI image with the near infrared band (b5) given a weight of

1.5, as this band is more effective in discriminating vegetated from less vegetated lava surfaces (Head et al., 2013; Li et al., 2015a), and the other bands a weight of 1. As the scale parameter proves to be the most important parameter (owing to its direct impact on classification accuracy by determining the size of image objects (Duro et al., 2012; Kim et al., 2008; Myint et al., 2011; Smith, 2010), it was decided to conduct tests with different values for the scale parameter in this study. A large value (0.9) was given to the color parameter and a very low (0.1) to the shape parameter, and equal values to the smoothness and compactness parameters. The reason for this parameter choice is that the interest of the classification in this study lies on lava flows of contrasting age, which show similarity in spectral behavior, so emphasis on the color parameter should potentially enhance the ability of differentiating between lava flows based on their spectral characteristics. In addition, lava flow are not expected to follow a systematic trend in shape nor, more importantly, need to be separated from other land covers exhibiting more regular shapes.

3.5 Object-based classification

A number of features can be extracted for each object after image segmentation and used as criteria for classification. In this study, over 100 features, like those used in (Demarchi et al., 2016), were selected for object-based random forest classification and grouped in different categories (Table 2). As previously mentioned, geometric information is considered less essential in the study of lava surfaces. Spectral and textural features, rather than geometric ones, were therefore highlighted. Topographic data were included for potential usefulness. It was expected that a large part of the features would be highly correlated, e.g. mean radiance in b1 (CA) and b2 (Blue), mean radiance in b5 (NIR) and mean NDVI. Using the previously mentioned approach, the number of features was reduced to 43 among which four were topographic features. In order to assess the usefulness of topographic data, object-based classification was performed with 43 features including topography and with 39 features excluding topography. Approximately 30% of the segments from each lava flow were selected as training samples for object-based classification.

Table 2 Input features for object-based random forest classification. For explanation of and calculation of the textural (on each layer of Landsat 8 OLI) and geometric features,

the reader is referred to Haralick (1979) and Trimble (2011). Std stands for standard deviation.

1. Landsat 8 data	2. Topography	3. Geometry	4. Texture (after Haralick)
Mean.b1 (Green)	Mean.Elevation; Std.Elevation	Area	Homogeneity (GLCM) for b1, b3-b7
Mean.b4 (Red); Std.b4	Mean.Slope	Compactness	Contrast (GLCM) for b3-b7
Std.b5 (NIR)	Mean.Aspect (Categorical)	Density	Angular 2nd moment (GLCM) for b5
Mean.b6 (SWIR1)			Mean (GLCM) for b3-b7
Mean.b7 (SWIR2); Std.b7			Std (GLCM) for b3-b7
Mean.NDVI; Std.NDVI			Angular 2nd moment (GLDV) for b2
Mean.BT; Std.BT			
Max.Diff			

3.6 Classification scenarios

Since classification of individual lava flows is difficult in such a complex lava field as Nyamuragira's, in this study classification was also performed for lava flows grouped by age. Using an interval of 4-5 years, the 20 lava flows were categorized into 8 groups (Table 3). The 1991-93 lava flow was treated as a single one-member group due to its unique physical and spectral characteristics (Li et al., 2015a).

Depending on the type of classification unit (pixel-based, object-based), the number of features used and the level of classification, eight different scenarios were defined in this study. By comparing them, it was expected to identify the best classification approach for mapping lava flows.

Table 3 Lava flow classes used in random forest classification.

Individual lava flows	Grouped lava flows
1958	1958
1967, 1971	1967-71

1976-77, 1980, 1981-82	1976-82
1984, 1986, 1989	1984-89
1991-93	1991-93
1994, 1996, 1998	1994-98
2000, 2001, 2002, 2004	2000-04
2006, 2010, 2011-12	2006-12
vegetation	vegetation

Table 4 Random forest classification scenarios defined in this study.

Scenario	Unit	Topographic features (Total number)	Level
1	Pixel-based	Yes (10)	Individual
2	Pixel-based	Yes (10)	Grouped
3	Pixel-based	No (7)	Individual
4	Pixel-based	No (7)	Grouped
5	Object-based	Yes (43)	Individual
6	Object-based	Yes (43)	Grouped
7	Object-based	No (39)	Individual
8	Object-based	No (39)	Grouped

3.7 Accuracy assessment

Reference data (Figure 2) used in the study were acquired in vector format (ArcGIS shapefile) from the Belgium's Royal Museum for Central Africa (Smets et al., 2010). Errors in the localization of lava flow edges due to vegetation recovery and manual drawing were estimated at less than one pixel of optical imagery and errors related to localizing vents and SAR data were not expected to significantly affect the results (Smets et al., 2010). Classification results of the study were compared with the reference data for accuracy assessment.

The accuracy assessment of both pixel- and object-based classification was conducted using a pixel-based approach (Whiteside et al., 2011). The advantages of the pixel-based approach are that it makes object-based and pixel-based classification results comparable and that quality of image segmentation is also indirectly considered. In order to better assess the accuracy of the classification results obtained, no post-classification processing was performed on the obtained classification maps. A total of 1840 pixels on the lava and vegetated surfaces, independent from

those used as training samples, were randomly selected from each lava flow and vegetated surface, based on the reference data. Accuracy assessment of classification was done by constructing confusion matrices and calculating commonly used accuracy assessment measures such as the overall accuracy (OA), producer's (PA) and user's accuracy (UA) for each class and Kappa coefficient (Congalton and Green, 2009). In order to determine whether the results of different classification scenarios are significantly different, a Z-test (Congalton and Green, 2009) was also applied in this study.

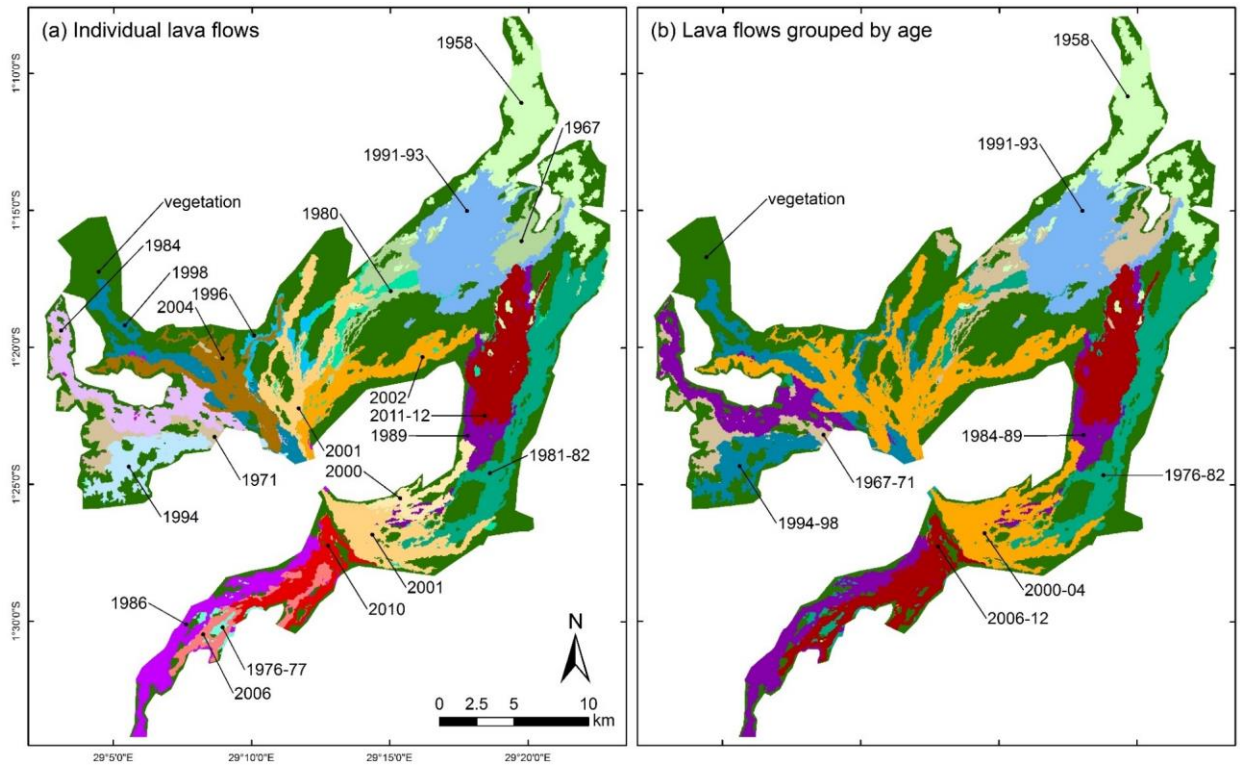

Figure 2 Reference data showing individual and grouped lava flows. The lava flows were obtained from Smets et al. (2010) and clipped in accordance with the area used for classification.

4 Results

4.1 Image segmentation

A range of scale parameter values were tested, yielding different numbers of segments. Smaller scale parameter values produced more lava segments (e.g. 2286 for SP = 10) and lava flows were

represented by many small segments. For larger scale parameter values, less segments were created (e.g. 516 for SP = 25), as lava flows were divided into bigger segments. A good scale parameter value should characterize lava flows with large segments but also capture smaller lava flows. Of the potential scale parameter values tested, 15 was considered most suitable in the study as it captures narrow lava flows and results in a total of 1157 segments (Figure 3).

4.2 Optimizing random forest parameters

Different values of the *ntree* and *mtry* parameters were tested to optimize random forest for each classification scenario. The candidate *ntree* values were varied from 500 to 5000 with increments of 500, while the candidate *mtry* values were 2 (half the default), 3 (the default) and 6 (twice the default) for the pixel-based classification and 4, 7 and 14 for the object-based classification, respectively. Figure 4 shows that with *ntree* = 2000 and *mtry* = 3, the lowest OOB error was obtained for Scenario 1. The OOB errors do not vary much for the parameter value pairs considered. OOB error seems to be more sensitive to *mtry* than to *ntree*. Optimal *ntree* and *mtry* parameter values for the other classification scenarios are listed in Table 5. Regarding the number of trees, the optimal value varies between 1000 and 4000. For the pixel-based classification, the default or half of the default value were selected as optimal for *mtry* while for the object-based classification the optimal mtry value was always equal to twice the default value.

Feature importance for each random forest was also assessed after the construction of random forests. For the pixel-based classification scenarios, NDVI proves to be the most important feature except for Scenario 2 (Figure 5a-d). The most significant difference between Scenarios 1 and 2 lies in the ranking of topographic feature importance: Aspect and Elevation are ranked immediately after NDVI in the former but are ranked before NDVI in the latter. After removing topographic features (Scenarios 3 and 4), the CA band and BT move to the first few positions.

Regarding the object-based classification scenarios (Table 2e-h), NDVI is the only feature that has an importance value >2. The classification scenarios using topographic features (Scenarios 5 and 6) have the same 12 features, the first nine of which are exactly in the same order of importance. In particular, both Elevation and Aspect features immediately follow NDVI in the importance rankings, similar to Scenarios 1 and 2. Without topographic features, BT has a higher importance rank in Scenarios 7 and 8 than in Scenarios 5 and 6. It is noted that textural features

are less dominant than spectral features. Geometric features were found to rank lowest among the features used for classification.

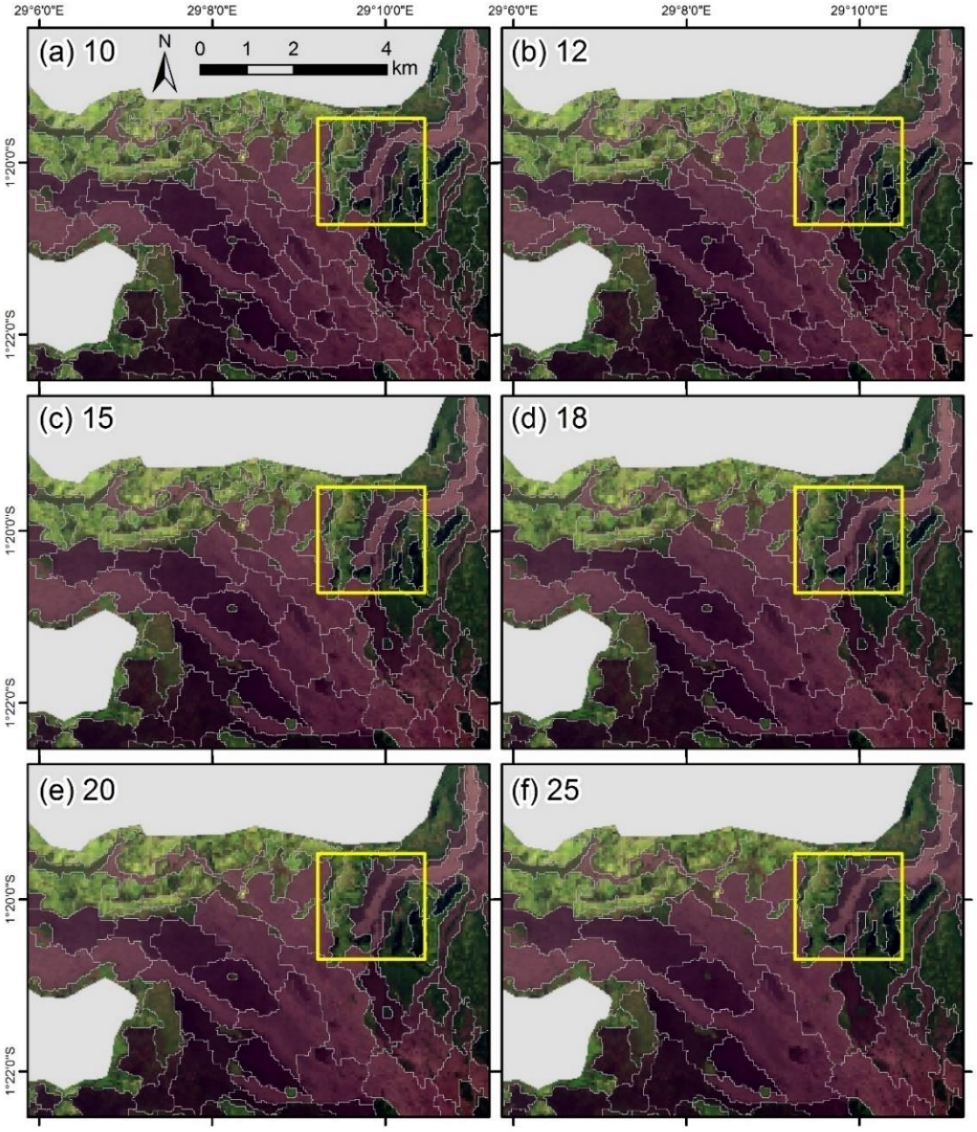

Figure 3 Image segmentation (partly shown for visibility) using various scale parameter values (SPs). The yellow squares highlight the major differences.

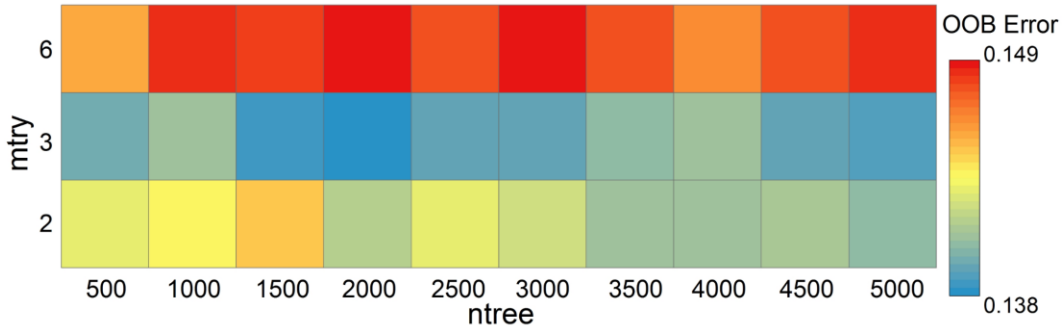

Figure 4 Matrix of OOB error for different parameters values of ntree and mtry for Scenario 1.

Table 5 Optimal ntree and mtry parameter values for all classification scenarios.

Scenario	*ntree*	*mtry*	Minimum OOB error
1	2000	3	0.1376
2	4000	2	0.0917
3	2000	3	0.2376
4	2500	2	0.1600
5	3000	14	0.2331
6	2500	14	0.1798
7	2000	14	0.3146
8	1000	14	0.2360

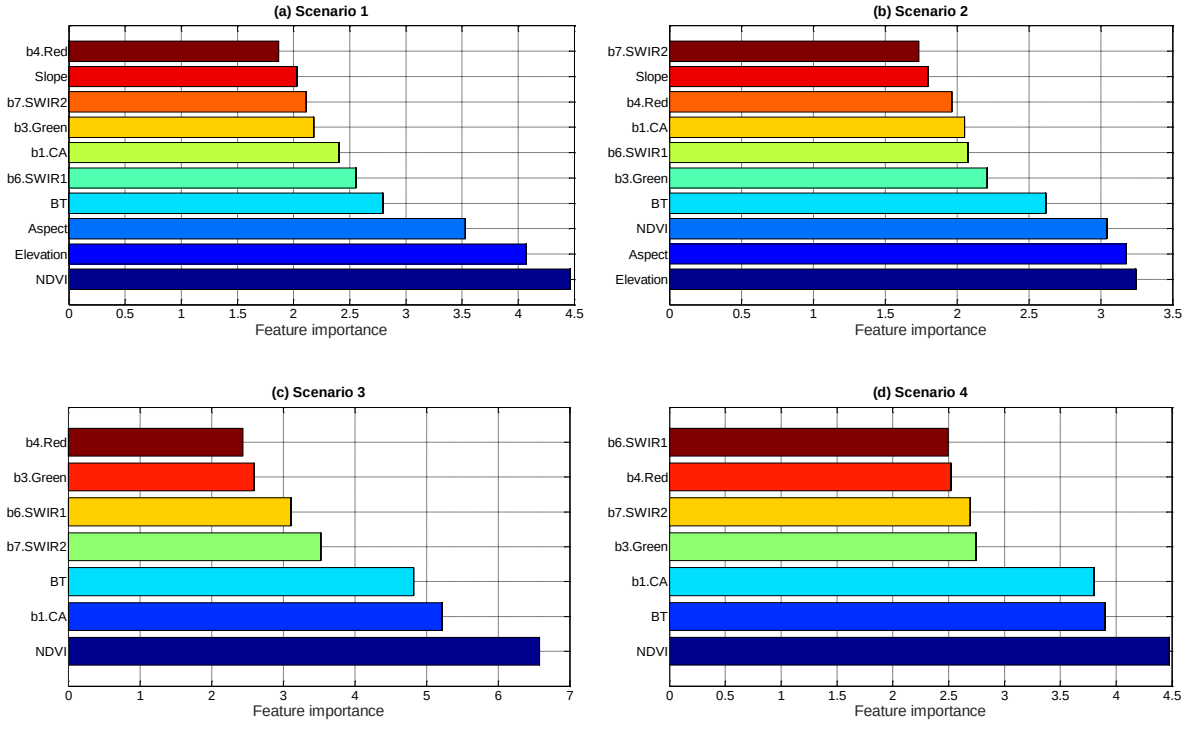

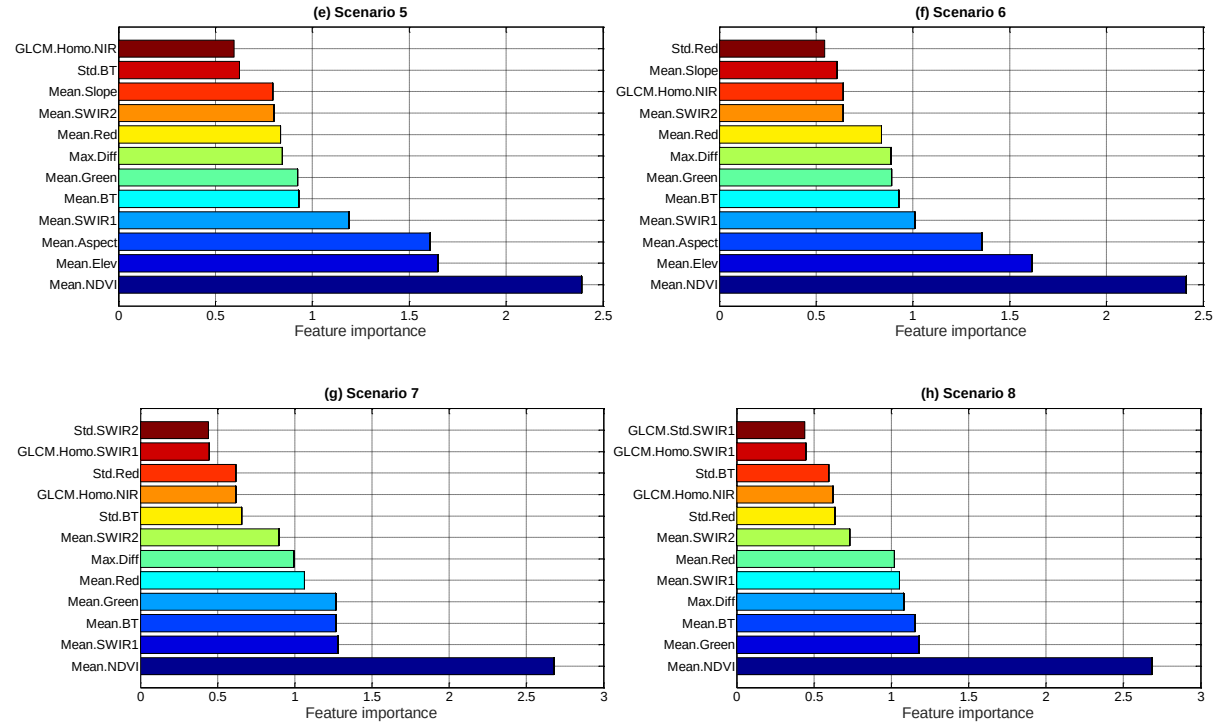

Figure 5 Normalized feature importance for different random forest classification scenarios. For the object-based random forest classification scenarios (e-h), only first 12 most important features are shown.

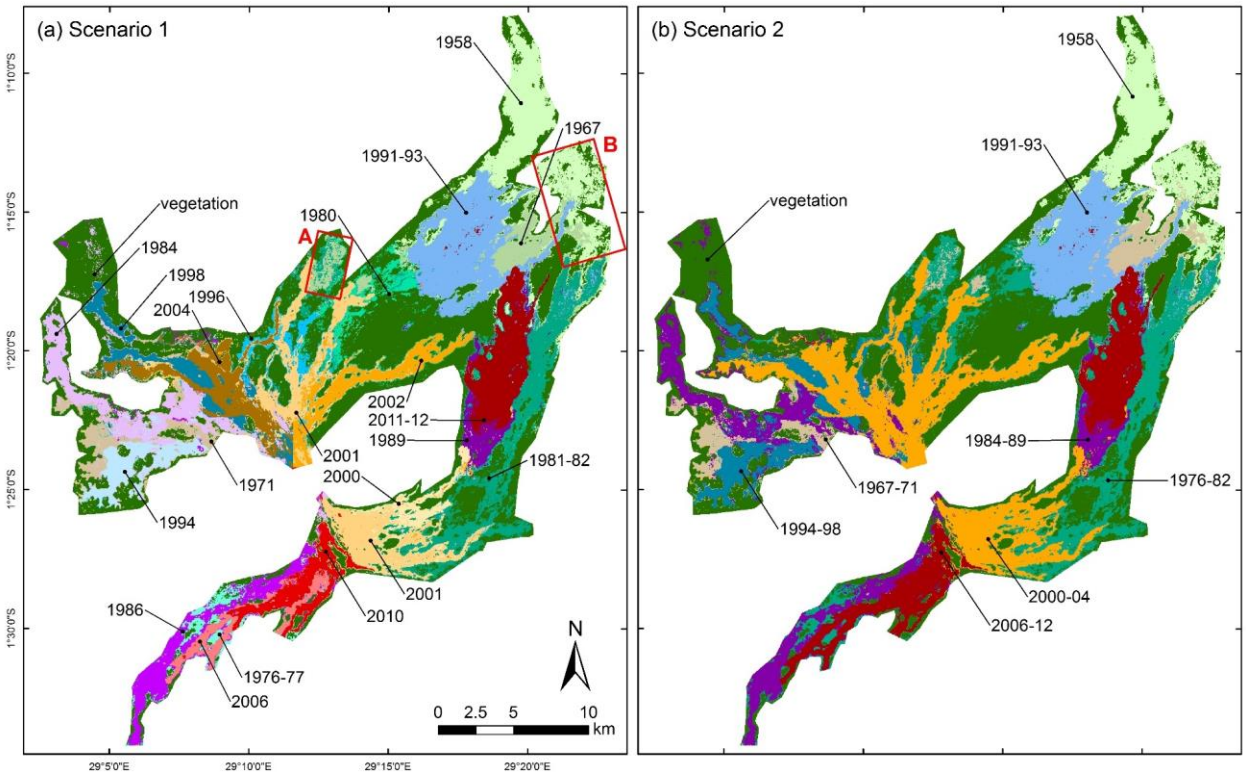

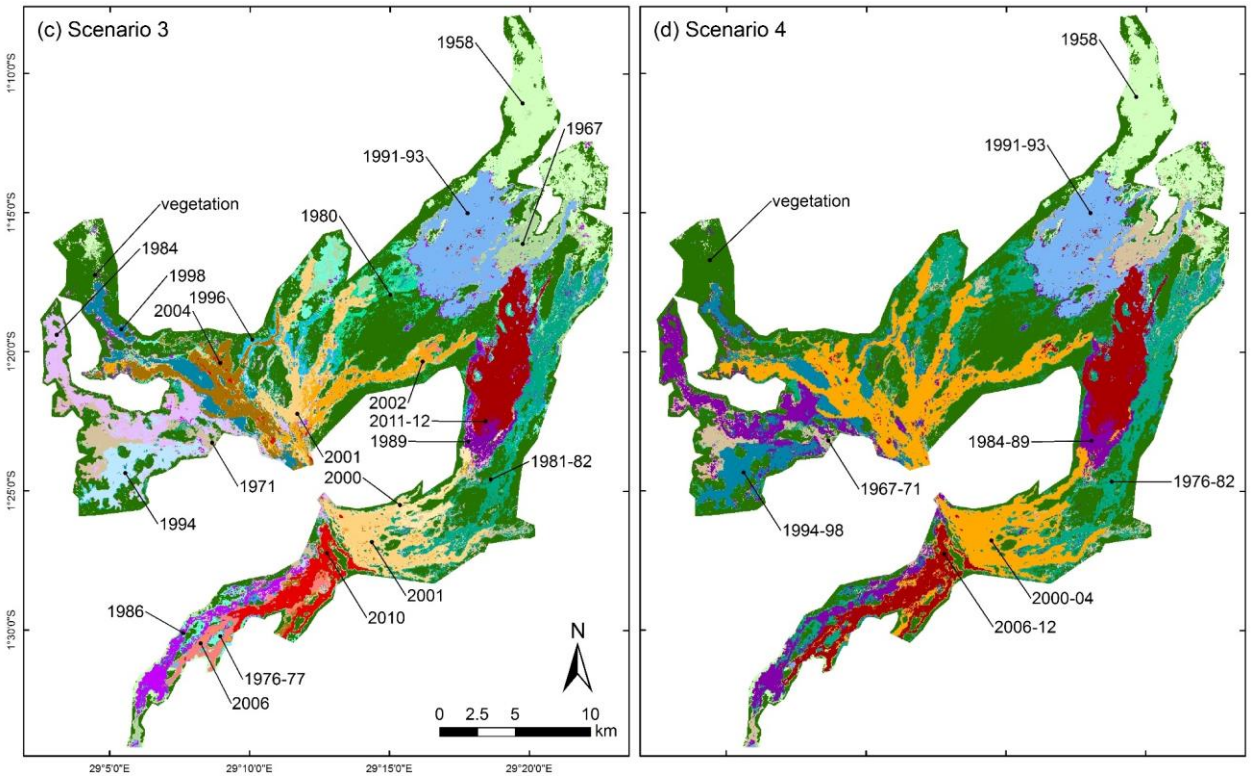
(c) Scenario 3
1958
1967
1991-93
vegetation
1980
1984
1998
1996
2004
2002
2011-12
1989
2001
2000
1981-82
1971
1994
2001
2010
1986
1976-77
2006
N
0 2.5 5 10
km
1°10'0"S
1°15'0"S
1°20'0"S
1°25'0"S
1°30'0"S
29°5'0"E
29°10'0"E
29°15'0"E
29°20'0"E
(d) Scenario 4
1958
1991-93
vegetation
1984-89
1976-82
1967-71
1994-98
2000-04
2006-12

363

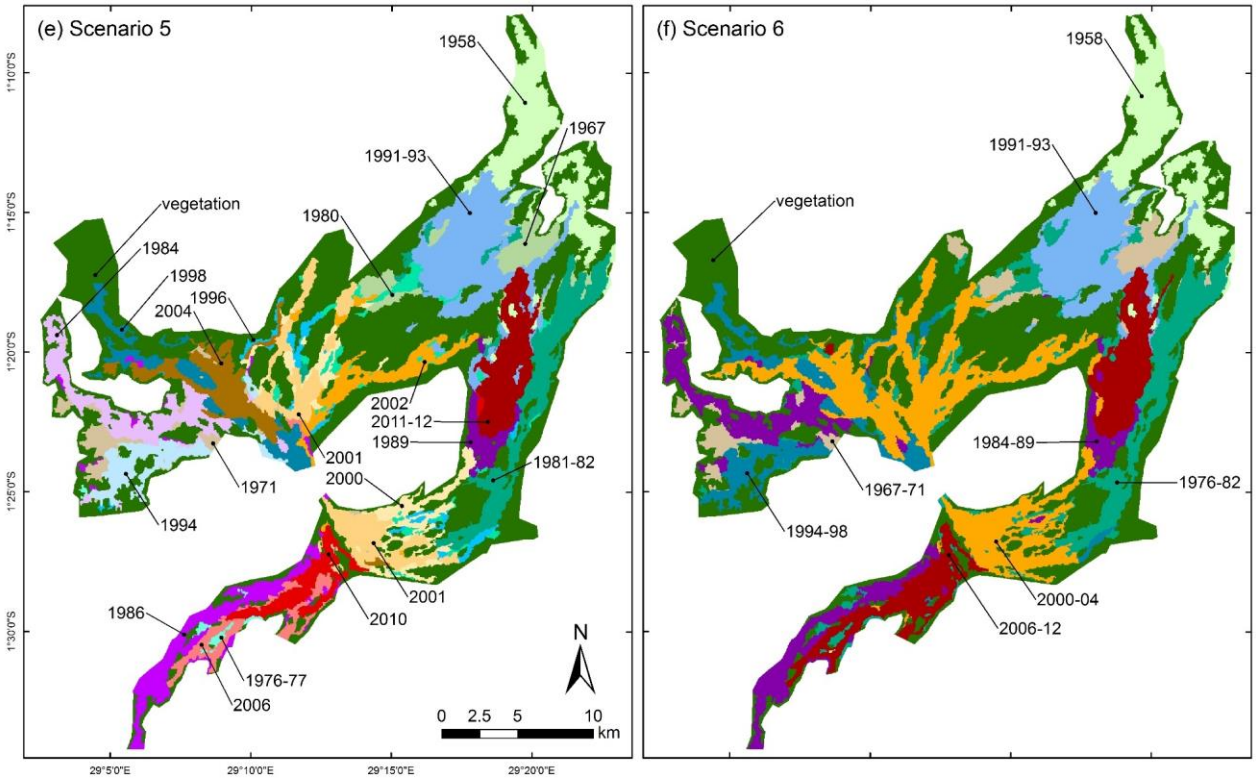
(e) Scenario 5
1958
1967
1991-93
vegetation
1980
1984
1998
1996
2004
2002
2011-12
1989
2001
2000
1981-82
1971
1994
2001
2010
1986
1976-77
2006
N
0 2.5 5 10
km
1°10'0"S
1°15'0"S
1°20'0"S
1°25'0"S
1°30'0"S
29°5'0"E
29°10'0"E
29°15'0"E
29°20'0"E
(f) Scenario 6
1958
1991-93
vegetation
1984-89
1976-82
1967-71
1994-98
2000-04
2006-12

364

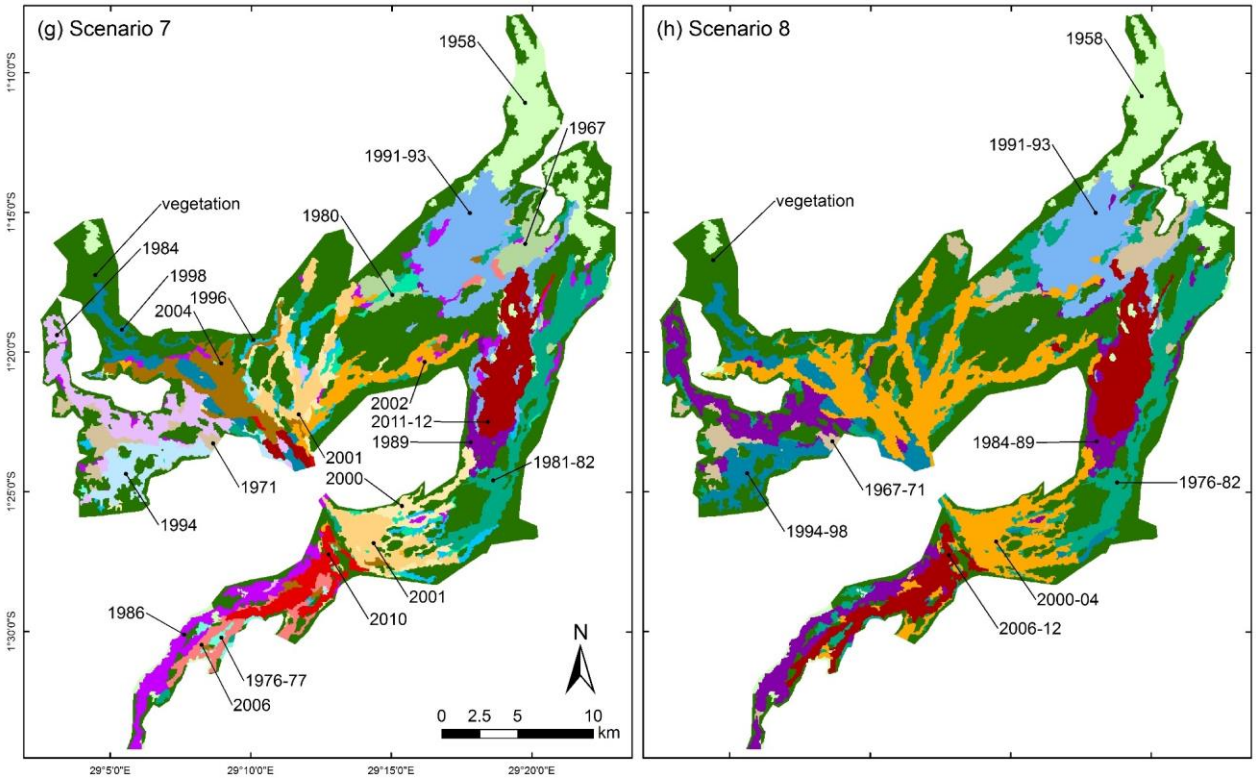

Figure 6 Classification results obtained through random forest for the different scenarios. The two red rectangles in (a) show the unknown lava surfaces mapped by the classification process.

4.3 Classification results

Through the random forests created above, classification was conducted for each scenario and the resultant maps are given in Figure 6. It is observed that pixel-based classification (Scenarios 1-4) produces lava surfaces that are more fragmented and heterogeneous with often ambiguous boundaries while object-based classification (Scenarios 5-8) results in more continuous and homogeneous lava units with clear boundaries. A good example is the 1986 lava flow (on the SW of the maps in Figure 6): it appears very fragmented on the pixel-based classification maps but is well discriminated and more complete on the object-based classification maps. The outcome of the classification of individual lava flows (Scenarios 1, 3, 5 and 7) is less homogenous than that of the classification of grouped lava flows (Scenarios 2, 4 ,6 and 8). Removal of topographic features leads to some differences in the maps when comparing the classification scenarios with or without topographic features (i.e. Scenarios 1 vs 3, Scenarios 2 vs 4, Scenarios 5 vs 7, and Scenarios 6 vs 8). It is also noted that the pixel-based classification is

more sensitive to unmapped lava surfaces than the object-based classification. These areas are not identified as recent lava flows in the reference map (Figure 2), e.g. the areas in the two red rectangles in Figure 6a, but are classified as part of the 1958 flow by the pixel-based scenarios.

4.4 Accuracy assessment

Producer's accuracies, user's accuracies, overall accuracies and Kappa coefficients for all classification scenarios are listed in Table 6 and Table 7. In general, classification accuracies for all scenarios are very good. It is clear that the classification of grouped lava flows has higher overall accuracies and higher Kappa coefficients than classification of individual lava flows regardless of the classification unit, as could have been expected. It is also interesting to note that pixel-based classification obtains higher overall accuracies and higher Kappa coefficients than object-based classification except for Scenarios 4 and 8. The difference in accuracy is most substantial between Scenarios 1 and 5 where individual lava flows are mapped considering topographic features. For pixel-based classification of both individual and grouped lava flows, removing topographic features leads to a decrease of >6% in overall accuracy while this decrease is however smaller for object-based classification (~2.5%).

The Z-tests (Table 8) were performed on different pairs of classification scenarios: comparison within the pixel-based (or object-based) classification can help to understand differences in accuracy between classification using topographic features or not. Comparison between pixel-based and object-based classification using the Z-tests can reveal which approach is best for mapping lava flows. Using topographic features significantly improves classification results except for object-based classification of individual lava flows. Pixel-based classification performs significantly better than its object-based counterpart except for classifying grouped lava flows without using topographic features.

For the pixel-based classification Scenarios 1 and 3 (Table 6), both producer's and user's accuracies are high for all the flows except for the 1989 and 1976-77 flows. The 1989 flow (PA = 0.48 for Scenario 1 and PA = 0.33 for Scenario 3 respectively) is largely misclassified as the neighboring 1981-82 flow (Figure 6a and c). The 1976-77 flow has a very high producer's accuracy but a very low user's accuracy (UA = 0.47 for Scenario 1 and UA = 0.31 for Scenario 3 respectively) because part of the neighboring 1989 flow is misclassified as the 1976-77 flow.

For classification Scenario 5 and 7 (Table 6), it is observed that the 1980, 1989, 1996 and 2001 flows have low producer's accuracies (<0.6) and that the 1980, 1996 and 2000 flows have low user's accuracies (<0.6). The 1980 flow is mostly confused with vegetation, while the 2001 flow is mostly confused with the 2000 flow (Figure 6e and Figure 6g).

Regarding the pixel-based random forest classification of grouped lava flows (Scenarios 2 and 4 in Table 7), all the producer's and user's accuracies are high (at least >0.76) for Scenario 2. For Scenario 4, the 1967-71 group (PA = 0.59) is mostly misclassified as the 1976-82 and 1984-89 groups (Figure 6d).

For classification Scenarios 6 and 8 (Table 7) show that all the flows have very similar accuracies in the two scenarios except for the 1958 flow group (increase by 12% in UA) and for the 1976-82 flow group (decrease by 11% in UA). It is noticed that the 1967-71 group is the most misclassified: it is confused with the 1984-89 group in Scenario 6 (Figure 6f) and with the 1976-82 and 1984-89 groups in Scenario 8 (Figure 6h).

Table 6 Accuracy assessment for classification of individual lava flows.

	Scenario 1		Scenario 3		Scenario 5		Scenario 7	
	PA	UA	PA	UA	PA	UA	PA	0.89
1958	0.87	0.91	0.85	0.89	0.85	0.87	0.85	0.77
1967	0.71	0.88	0.62	0.76	0.60	0.71	0.64	0.97
1971	0.84	0.79	0.7	0.60	0.70	0.94	0.66	0.89
1976-77	1.00	**0.47**	0.89	**0.31**	0.67	0.86	0.89	**0.47**
1980	0.70	0.78	0.63	0.58	0.5	**0.49**	**0.45**	0.74
1981-82	0.88	0.78	0.75	0.67	0.83	0.89	0.79	0.82
1984	0.86	0.84	0.81	0.71	0.94	0.84	0.94	0.76
1986	0.85	0.97	0.68	0.86	0.99	0.87	0.89	0.92
1989	**0.48**	0.88	**0.33**	0.79	**0.50**	0.92	**0.48**	0.84
1991-93	0.98	0.93	0.94	0.85	1.00	0.86	0.90	0.84
1994	0.91	0.89	0.84	0.82	0.9	0.86	0.90	**0.44**
1996	0.89	0.84	0.77	0.73	**0.53**	**0.53**	**0.55**	0.91
1998	0.90	0.91	0.75	0.89	0.84	0.73	0.75	0.43
2000	0.79	0.71	0.67	0.70	0.90	0.39	0.89	0.89
2001	0.85	0.86	0.83	0.81	**0.56**	0.88	**0.55**	0.85

2002	0.88	0.88	0.73	0.71	0.77	0.85	0.73	0.83
2004	0.93	0.97	0.88	0.92	0.86	0.94	0.84	0.77
2006	0.88	0.93	0.64	0.82	0.88	0.79	0.75	0.90
2010	0.97	0.94	0.96	0.88	0.87	0.92	0.86	0.75
2011-12	0.99	1.00	0.96	0.97	0.91	0.99	0.91	0.66
vegetation	0.95	0.85	0.90	0.85	0.90	0.66	0.91	0.89
OA	87.66%		79.51%		78.86%		76.36%	
Kappa	0.8679		0.7804		0.7750		0.7484	

425 *Table 7 Accuracy assessment for classification of grouped lava flows. Scenarios 4b and 8b*
426 *are new scenarios introduced in Section 5.2.2.*

	Scenario 2		Scenario 4		Scenario 6		Scenario 8		Scenario 4b		Scenario 8b	
	PA	UA	PA	UA	PA	UA	PA	UA	PA	UA	PA	UA
1958	0.83	0.93	0.87	0.93	0.85	0.87	0.85	0.87	0.85	0.89	0.85	1
1967-71	0.77	0.84	**0.59**	0.71	0.60	0.84	0.60	0.84	0.65	0.6	0.64	0.74
1976-82	0.91	0.78	0.82	0.63	0.80	0.72	0.80	0.72	0.8	**0.48**	0.75	**0.44**
1984-89	0.76	0.88	0.69	0.80	0.85	0.88	0.85	0.88	**0.52**	0.77	0.63	0.85
1991-93	0.97	0.95	0.93	0.88	0.97	0.94	0.97	0.94	0.95	0.63	0.95	0.73
1994-98	0.86	0.90	0.78	0.87	0.80	0.90	0.80	0.90	0.69	0.76	0.67	0.88
2000-04	0.97	0.95	0.94	0.89	0.95	0.95	0.95	0.95	0.8	0.83	0.79	0.76
2006-12	0.98	0.98	0.84	0.93	0.97	0.98	0.97	0.98	0.65	0.85	**0.53**	0.78
vegetation	0.95	0.87	0.89	0.86	0.90	0.68	0.90	0.68	0.93	0.8	0.91	0.6
OA	91.25%		84.57%		88.97%		86.47%		74.29%		72.45%	
Kappa	0.8924		0.8098		0.8647		0.8334		0.6878		0.6632	

427 *Table 8 Kappa analysis of significance (at the 95% confidence level) for comparing*
428 *accuracies for different classification scenarios.*

	Comparison	*Z* statistic	*p* value	Result
A: Pixel-based	Scenarios 1 vs 3	6.7373	<0.001	Significantly different
	Scenarios 2 vs 4	6.3411	<0.001	Significantly different
B: Object-based	Scenarios 5 vs 7	1.8213	0.0686	**Not** significantly different
	Scenarios 6 vs 8	2.3788	0.0174	Significantly different
C: Pixel-based	Scenarios 1 vs 5	7.1288	<0.001	Significantly different
vs Object-based	Scenarios 2 vs 6	2.3213	0.0203	Significantly different
	Scenarios 3 vs 7	2.2006	0.0278	Significantly different

Scenarios 4 vs 8	1.6683	0.0953	**Not** significantly different

5 Discussion

In this study, pixel-based and object-based random forest classification was carried out in order to classify both individual and grouped lava flows from Nyamuragira using Landsat 8 imagery with topographic variables being used as optional ancillary data. As a result, eight different classification scenarios were defined (Table 4). The lava flow map by Smets et al. (2010) was used to assess the quality of classification results produced by the method presented in the study. The classification results show a good level of accuracy in discriminating individual and grouped lava flows, with pixel-based classification performing mostly significantly better than its object-based counterpart.

However, the object-based image segmentation can serve as an interesting tool to separate lava flows of contrasting spectral and textural characteristics and such potential has been demonstrated in previous studies of mapping volcanic deposits including lava flows (Kassouk et al., 2014; Thouret et al., 2015). In order to illustrate its applicability, image segmentation is also tested here on Fernandina Island, which is an active shield volcano of Ecuador's Galápagos Islands in the Pacific Ocean (Figure 7) with a summit elevation of 1476 meters and multiple eruptions recorded in the last century (Smithsonian Institution, 2013). Result of image segmentation which is based on the datasets of Fernandina, similar to those of Nyamuragira, reveals that lava flow surfaces of contrasting colors are separated (Figure 7). Due to a lack of lava age information used for calibration, we are not able to run random forest classification in the case of Fernandina. As such, we highlight that supervised random forest classification of lava flow surfaces into homogenous (age) groups does require the availability of sufficient field knowledge to train the classifier—this is a prerequisite of supervised classification and particularly a need of discriminating of many spatially overlapping and spectrally similar lava flows. However, the reference data—which is a good lava flow map produced by Smets et al. (2010) in our study—does not need to be a complete lava flow map to provide training and validation samples. It is noted that this study does not intend to focus on dating lava flows through remote sensing image classification while how spectral information of lava flows can be

used to assess the age of lava flows is presented in other complementary articles (Li et al., 2015a, 2015b, 2017 (in prep.)).

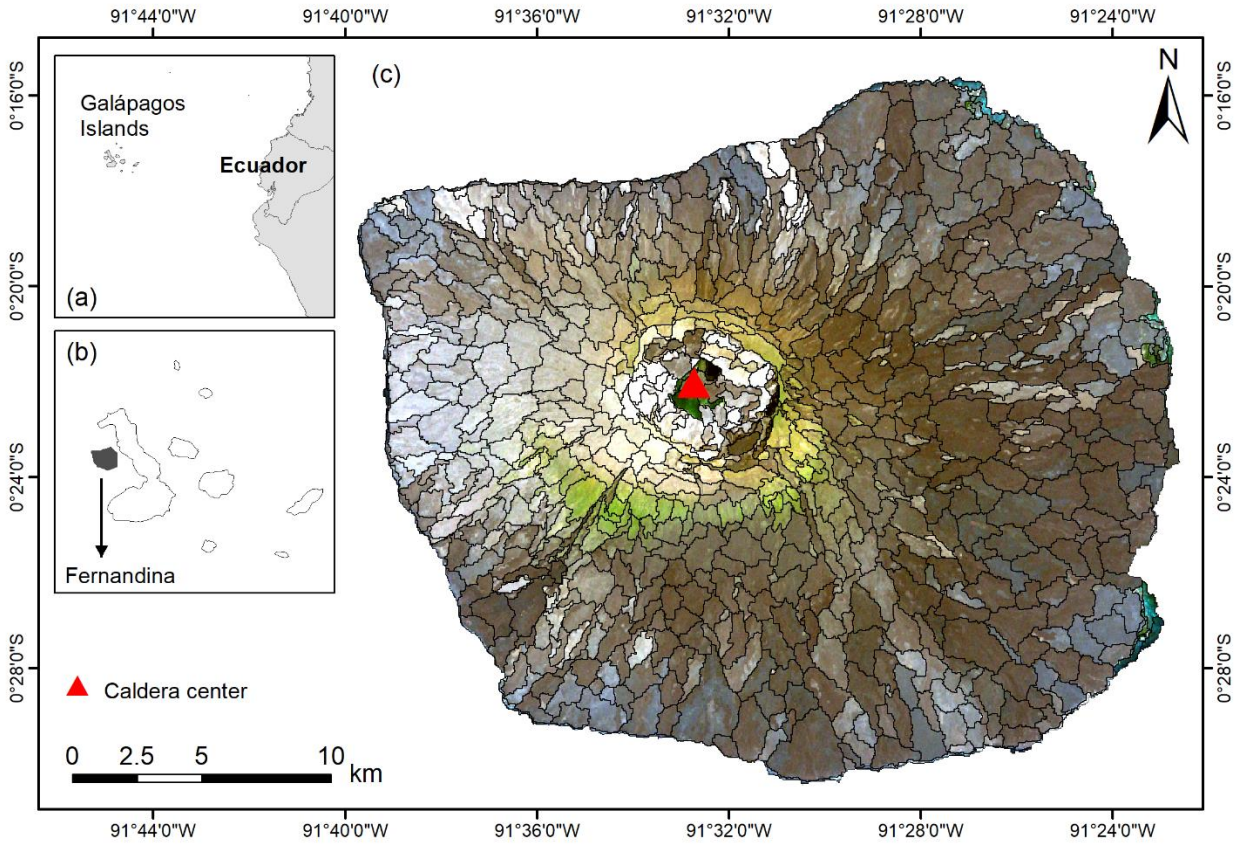

Figure 7 Image segmentation for Fernandina Island (Ecuador) based on datasets including a Landsat 7 ETM+ image (acquired on Oct-26-2001) and 30-meter SRTM DEM data. With the scale parameter being set at 15, lava flow surfaces of contrasting colors are discriminated through image segmentation.

5.1 Interpretation of feature importance

Following previous research (Eisavi et al., 2015; Gislason et al., 2006; Vaglio Laurin et al., 2014), this study paid attention to parameterization of the random forest algorithm used in this study. In fact, it is shown that changing in *ntree* and *mtry* parameter values does not result in a substantial differences in OOB error, agreeing with the findings from other studies (Gislason et al., 2006; Liaw and Wiener, 2002). A smaller optimal *mtry* value for the pixel-based classification scenarios, but a larger *mtry* value for the object-based ones suggests that a larger

mtry is more suitable if there is a larger number of features, a point already noted by other researchers (Liaw and Wiener, 2002).

Random forest grows a number of decision trees by means of bagging (bootstrap aggregating), a type of ensemble classification methods which are generally considered to be black-box classifiers (Gislason et al., 2006). This makes interpretation of random forest quite complex but the feature importance returned by the random forest classifier is very useful for a better understanding of the classification outcome. For most of the classification runs in this study, NDVI is ranked first among the features, which highlights its important role in discriminating lava flows of different age. This is consistent with the observation of reflectance in NIR for Nyamuragira's lava flows (Head et al., 2013), and with the relationships of lava flow age with vegetation fraction (Li et al., 2015a).

From the ranking of feature importance for the four object-based classification scenarios, textural features prove to be less important than spectral features, which can be explained by textural similarity between different lava flows. It suggests that at the Landsat 30 m resolution textural features are not that useful for mapping lava flows. Given the ranking of geometric features, they do not seem to play an essential role in lava flow classification. More discussion about the texture and geometry of objects will be provided in the next section.

For classification scenarios including topography, Elevation and Aspect are also found to be highly ranked, particularly for Scenario 2. Concerning the role of topography in classification of lava flows, coupled with its effect on classification accuracy, a detailed analysis is given in Section 5.2. When topographic features are removed, BT is higher ranked. Lava flows completely cool down in days to years (<5 years) even if they are thick. The increased ranking of BT after the removal of topographic features is therefore not attributed to actual difference in temperature related to the heat from lava emplacement, but is rather to the variability in lava emissivity. Lava surface emissivity is controlled by multiple factors which can be broadly categorized into two groups: those explaining an initial difference in emissivity between (or within) lava flow fields (e.g. lava surface texture) and those responsible for later emissivity differences as time elapses (i.e. aging factors such as weathering and vegetation) (Byrnes et al., 2004; Kahle et al., 1988; Li et al., 2015b). Particularly, initial lava surface textures have been shown to vary within individual lava flows although this cannot be revealed in a DEM dataset at

30 meters, and the textual contrast can be partly correlated to change in slope or elevation (i.e. distance from the vent) (Byrnes and Crown, 2001; Murcia et al., 2014). Despite rough a'a being the main lava morphology type at Nyamuragira, surface roughness of lava flows is modified to some extent as a result of ash fall from later eruptions and weathering products. Chemical weathering changes the color of lava surfaces from dark to yellow/red (Li et al., 2015b) and thus changes lava emissivity (Kahle et al., 1988). In addition, the coverage of lichens and vegetation on the lava flow surfaces also contributes to the variations in lava emissivity.

5.2 Comparison of classification scenarios

5.2.1 Role of topographic features

In terms of feature importance, topographic features, notably Elevation and Aspect, are identified as highly important. In most cases, they help to improve classification accuracies significantly, except for object-based classification of individual lava flows. The initial purpose of taking topography into account was the expectation that topographic features would correct for the variation in spectra observed within single lava flows due to elevation (as elevation impacts vegetation recovery on lava surfaces), but it seems that random forest just groups pixels or objects of similar elevation and aspect together.

In general, elevation is used to support classification because it is known that certain classes have certain heights or exist at certain elevations, e.g. contrasting heights between buildings and roads (Li and Shao, 2014) and altitudinal zonation of vegetation on mountains (Ma et al., 2015). In our case study, there is no definite relationship between elevation and lava flow age. A single lava flow however tends to occur on a specific flank and within a limited elevation range in the case of Nyamuragira. Random forest treats all the input features equally—whether or not they are meaningful—selects part of them at random for growing trees, and only considers the features that return lower OOB errors as more important features. As a consequence, to some extent including topographic features in random forest classification for mapping lava flows is appropriate as it increases the chance of pixel/objects located on the same flank orientation and at similar elevation to be attributed to the same class, which is consistent with the emplacement of lava flows. This explains the higher accuracies returned by the classification scenarios including these topographic features. For the classification of lava flow age groups, this might be

less valid as different lava flows within a given time period are emitted from different vents. Nevertheless, it is reported that due to the evolution of the magmatic system, the location of eruption evolved in a non-random way over time at Nyamuragira (Smets et al., 2015): eruptions often occurred at the foot of the central edifice between 1938 and 1994 but in the caldera or along the upper flanks afterwards. This might explain why elevation is a significant factor for classifying lava age groups as well.

In order to further understand the role that topographic features play in the classification carried out in this study, a consequent future line of investigation would be to explore if topographic features remain important when applying the same classification approach on other volcanoes where lava flows have similar elevation ranges and branches of the same lava flow are distributed on different flanks of the volcano.

5.2.2 Individual vs grouped lava flows

Classification of grouped lava flows results in higher classification accuracies than classification of individual lava flows. By combining samples for 20 individual lava flow classes to create samples for eight grouped lava flow classes, in fact we aimed at decreasing the spectral confusion between lava flows of similar age, e. g. the 2000, 2001 and 2002 lava flows. As such, it is logical that overall classification accuracies are improved.

It is acknowledged that from a volcanological point of view it is more interesting to map individual lava flows for a volcano, but this is very often problematic as lava flows may be erupted within a short period of time, some eruptions consist of several phases of activity, separated by short repose phases, and can be more complicated to map if flows overlap. This means that mapping lava flows grouped by similar age is a good compromise. Such an approach using age groups is also relevant for volcanoes for which no, or a limited number of, lava flows have been dated. Flows can then be labelled as broad age groups and less detailed training data will be required to perform the mapping. To test this capability, new classification scenarios based on Scenarios 4 and 8—only scenarios without using topography are tested as a demonstration case here—were defined as Scenarios 4b and 8b, for mapping grouped lava flows based on limited ground truth, assuming the existence of some undated lava flows. For the groups consisting of at least three main flows, one lava flow (or two) was not sampled for

558 classification: the 1980 flow in the 1976-82 group, the 1986 in the 1984-89, the 1996 in the
559 1994-98, the 2001 and 2002 in the 2000-04 and the 2010 in the 2006-12.

560 After determination of optimal values for parameters *ntree* and *mtry*, random forest classification
561 was carried out for classifying grouped lava flows at both pixel and object scales. Accuracy
562 assessment (based on the same validation datasets as the other scenarios) shows that
563 classification of grouped lava flows with some of the individual flows omitted for sampling
564 performs acceptably (see accuracy assessment in Table 7), although the accuracy measures are
565 significantly lower than for Scenarios 4 and 8 with all lava flows used in the calibration. Similar
566 to Scenarios 4 and 8, the overall accuracies and Kappa coefficients of the two new scenarios are
567 very close and the Z test further confirms that the two new classification scenarios are not
568 significantly different from each other (Table 9). The classification maps (Figure 8) show that
569 the flow groups with one or two lava flows not sampled are generally more misclassified than the
570 groups with all flows used for training. It is clear that in the pixel-based Scenario 4b and object-
571 based Scenario 8b, the 1986 flow in the 1984-1989 group is largely misclassified as being part of
572 the 1976-82 group, the 1996 flow in the 1994-98 group as being part of the 2000-04 group, and
573 the 2010 flow in the 2006-12 group as being part of the 2000-04 group. This first test suggests
574 that it is possible, to a certain extent, to map grouped lava flows by allocating unknown/undated
575 flow surfaces to a lava flow group and that somehow this approach can be used as an alternative
576 age estimation technique. However, the results presented need to be interpreted with caution as
577 accuracies are reduced for undated flows and confusion arise, especially for fresh flows.

578 Although the performance of the new classification scenarios is slightly lower than the fully
579 calibrated ones, this test demonstrates the possibility of associating a lava surface of unknown
580 age to a group of flow of known age. However, it is noted that for the presented approach to be
581 used, field knowledge or expert judgment is required to start grouping lava flows of similar age.

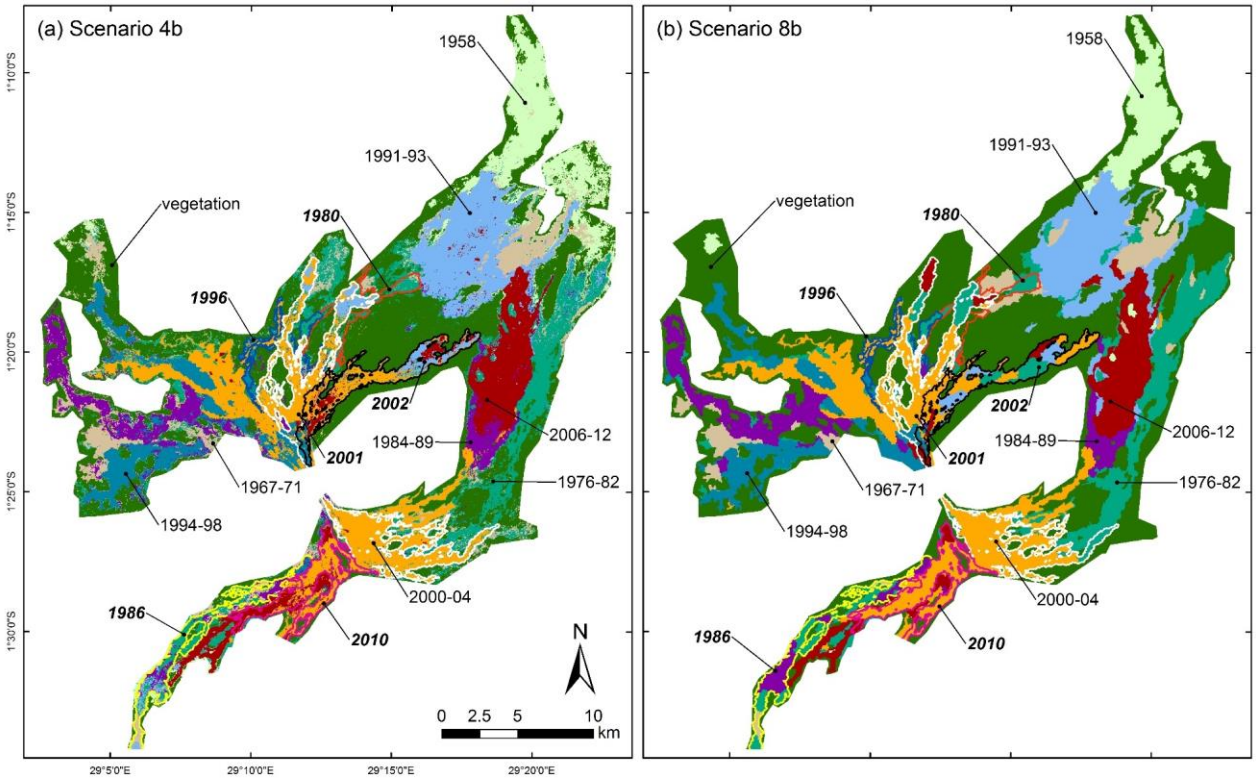

Figure 8 Classification results for pixel-based Scenario 4b and object-based Scenario 8b, defined to evaluate the accuracy of mapping grouped lava flows without sampling every individual lava flow.

Table 9 Accuracy assessment for the outcome of the pixel-based Scenario 4b and object-based Scenario 8b for mapping grouped lava flows

New scenario	Parameters for random forest	Overall accuracy	Kappa coefficient	Z static (p)
4b (pixel-based)	*ntree* = 2000 *mtry* = 3	0.7429	0.6878	$Z = 1.3922$ $p = 0.1639$
8b (object-based)	*ntree* = 1000 *mtry* = 7	0.7245	0.6632	Not significantly different

5.2.3 Pixel-based vs object-based classification

No researchers so far have attempted to map Nyamuragira's lava flows using image classification except for Head et al. (2013) who claimed that pixel-based supervised classification was less successful and used pixel-based unsupervised classification (ISODATA) followed by manual editing. As these authors did not report classification accuracies, it is impossible to compare our results with their study.

Kappa analysis in this study shows that pixel-based and object-based random forest classification produces significantly different results in terms of classification accuracy. Pixel-based classification of lava flows returns higher accuracy values than object-based classification, except for mapping lava flows age groups without using topographic features. A number of earlier studies (Blaschke, 2010; Ouyang et al., 2011; Whiteside et al., 2011) have shown that object-based classification outperforms pixel-based classification, but it is noted that most of these studies are not comparing "like by like" and often use different classifiers, e.g. pixel-based Maximum Likelihood classifier vs object-based Nearest Neighbor classifier (Ouyang et al., 2011). This makes it difficult to draw a conclusion such as that object-based classification is superior to pixel-based classification. This study suggests that object-based classification is not necessarily better than pixel-based classification when random forest classifier is used. This agrees with Duro et al. (2012) who reach the conclusion that no statistical difference exists between pixel-based and object-based classification when using machine learning classifiers such as support vector machines, decision tree and random forest.

It has been widely recognized that one of the advantages of object-based classification compared to pixel-based classification is the possibility of including geometric and textural information related to objects in the classification process. In this study, geometric features and many textural features were extracted for random forest classification but it was found that they are not really important in comparison with spectral features for classifying lava flows (Figure 5). As mentioned earlier in Section 3.4, this is because lava flow objects corresponding to different lava flows do not have discriminating shapes. With respect to textural features, lava flows of different age show limited variance between each other. As a result, the typical advantages of object-based classification do not effectively contribute to mapping lava flows. This may explain why object-based classification is not superior to pixel-based classification in this study.

Also image segmentation may strongly affect the accuracy of object-classification. When the pixel-based accuracy assessment approach is used for object-based classification, it actually takes two aspects of object-based classification accuracy into account: the accuracy of the image classification process itself and the accuracy of image segmentation (e.g. two validation pixels within one object might belong to two different lava flows). In this study, the scale parameter used is definitely appropriate, as it partitioned objects along the lava flow edges, but it would

also be worth experimenting with smaller object sizes (rather than larger one as they tend to decrease the segmentation accuracies (Liu and Xia, 2010)). This might be a possible step to further improve the accuracy of object-based classification.

Although in this study object-based classification does not seem to have clear advantages over the pixel-based approach in terms of classification accuracy, it is clear that the pixel-based classification output suffers from the so-called "salt and pepper noise" while object-based classification output is more homogenous and therefore also more visually appealing. As the segmentation process is driven by the identification of spectral contrasts at the boundaries between flows, object-based classification results in maps more clearly delineating the actual boundary of flow units, even though some objects are misclassified. The results of object-based classification are also in vector format and hence readily available for spatial analysis on hazard assessment in vector-based GIS. Moreover, manual post-classification processing is quite easy for the object-based classification and this has the potential to improve the results significantly (Barraud, 2006; Tarquini and Favalli, 2010).

6 Conclusions

This study reviews previous studies on remote sensing mapping of lava flows in terms of data and methods and also gives a brief introduction to the mapping history of Nyamuragira volcano. Using pixel-based and object-based random forest classification, this study aims at identifying individual and grouped lava flows from a single Landsat 8 scene supported by DEM data. From the results, it is concluded that:

- Feature importance analysis shows that, in most cases, NDVI is the most important feature to distinguish lava flows of different age, immediately followed by topographic features if they are included in the classification. For object-based classification, textural features are ranked low while geometric features proved the least useful.
- Using topographic features of lava flows in random forest classification tend to improve classification significantly.
- Mapping lava flows grouped by age improves the accuracies of both pixel-based and object-based classification compared to mapping individual lava flows.

- Both pixel- and object-based classification performs well for mapping lava flows. Pixel-based classification results in significantly improved accuracy compared with object-based classification, indicating object-based classification does not necessarily outperform pixel-based classification when a machining learning classifier is used. Pixel-based classification results in heterogeneous and fragmental lava surfaces with "salt and pepper noise" while object-based classification produces homogeneous and continuous lava flows, which is more visually appealing. This is because that image segmentation can partition the satellite image, through spectral characteristics, into physically meaningful objects which in agreement with the shape of lava flows.

This study applies for the first time a machine learning classification approach to mapping lava flows, with both pixel-based and object-based classification being tested. Lava flows on a tropical volcano are successfully classified and discriminated from one single satellite image, in spite of spatial overlap, vegetation cover and similar age, and thus similar spectral characteristics. It is very likely that accuracy will be improved further if multiple-temporal images are used. This study also highlights that random forest classification can be used for mapping unmapped or poorly mapped volcanoes whose lava flows are not fully vegetated, but it requires certain spectral contrast between lava flows and their surrounding and between overlapping lava flows, as well as background knowledge for calibration.

For developing countries, particularly in Africa, radar images and archived documents might not be frequently freely available, but optical multispectral satellite images such as TM, ETM+, OLI, ALI and, more recently, Sentinel 2 are freely accessible through the Internet. As such, this study provides local researchers with low-cost, fast mapping approaches that require relatively minimal resources, for rapid update of maps after new lava flows, for accuracy assessment of existing lava flow maps and for lava flow hazard assessment.

Acknowledgements

Long Li wishes to thank the China Scholarship Council for supporting his research work at the Vrije Universiteit Brussel. This study contributes to a project funded by the Priority Academic Program Development of Jiangsu Higher Education Institutions (Surveying and Mapping Science and Technology discipline).

Reference

Abrams, M., Abbott, E., Kahle, A., 1991. Combined use of visible, reflected infrared, and thermal infrared images for mapping Hawaiian lava flows. J. Geophys. Res. 96, 475–484. doi:10.1029/90JB01392

Abrams, M., Bianchi, R., Pieri, D., 1996. Revised mapping of lava flows on Mount Etna, Sicily. Photogramm. Eng. Remote Sensing 62, 1353–1359. doi:10.1.1.30.4807

Albino, F., Smets, B., D'Oreye, N., Kervyn, F., 2015. High-resolution TanDEM-X DEM: An accurate method to estimate lava flow volumes at Nyamulagira Volcano (D. R. Congo). J. Geophys. Res. Solid Earth 120, 4189–4207. doi:10.1002/2015JB011988

Aufaristama, M., Höskuldsson, A., Jónsdóttir, I., Ólafsdóttir, R., 2016. Mapping and assessing surface morphology of Holocene Lava field in Krafla (NE Iceland) using hyperspectral remote sensing. IOP Conf. Ser. Earth Environ. Sci. 29, 12002. doi:10.1088/1755-1315/29/1/012002

Barraud, J., 2006. The use of watershed segmentation and GIS software for textural analysis of thin sections. J. Volcanol. Geotherm. Res. 154, 17–33. doi:10.1016/j.jvolgeores.2005.09.017

Belgiu, M., Drăguţ, L., 2016. Random forest in remote sensing: A review of applications and future directions. ISPRS J. Photogramm. Remote Sens. 114, 24–31. doi:10.1016/j.isprsjprs.2016.01.011

Blackett, M., 2014. Early analysis of Landsat-8 thermal infrared sensor imagery of volcanic activity. Remote Sens. 6, 2282–2295. doi:10.3390/rs6032282

Blaschke, T., 2010. Object based image analysis for remote sensing. ISPRS J. Photogramm. Remote Sens. 65, 2–16. doi:10.1016/j.isprsjprs.2009.06.004

Blaschke, T., Hay, G.J., Kelly, M., Lang, S., Hofmann, P., Addink, E., Queiroz Feitosa, R., Van Der Meer, F., Van Der Werff, H., Van Coillie, F., Tiede, D., 2014. Geographic Object-Based Image Analysis – Towards a new paradigm. ISPRS J. Photogramm. Remote Sens. 87, 180–191. doi:10.1016/j.isprsjprs.2013.09.014

Boulesteix, A.-L., Janitza, S., Kruppa, J., König, I.R., 2012. Overview of random forest methodology and practical guidance with emphasis on computational biology and bioinformatics. Wiley Interdiscip. Rev. Data Min. Knowl. Discov. 2, 493–507. doi:10.1002/widm.1072

Breiman, L., 2001. Random forests. Mach. Learn. 45, 5–32. doi:10.1023/A:1010933404324

Byrnes, J.M., Crown, D.A., 2001. Relationships between pahoehoe surface units, topography, and lava tubes at Mauna Ulu, Kilauea Volcano, Hawaii. J. Geophys. Res. Solid Earth 106, 2139–2151. doi:10.1029/2000JB900369

Byrnes, J.M., Ramsey, M.S., Crown, D.A., 2004. Surface unit characterization of the Mauna Ulu flow field, Kilauea Volcano, Hawai'i, using integrated field and remote sensing analyses. J. Volcanol. Geotherm. Res. 135, 169–193. doi:10.1016/j.jvolgeores.2003.12.016

Colclough, S., 2006. Investigations of Nyamuragira and Nyiragongo volcanoes (Democratic Republic of the Congo) using InSAR, in: Lacoste, H., Ouwehand, L. (Eds.), Fringe 2005 Workshop. European Space Agency, Frascati, Italy, pp. 1–6. doi:2006ESASP.610E..55C

Congalton, R.G., Green, K., 2009. Assessing the Accuracy of Remotely Sensed Data: Principles and Practices, 2nd ed. CRC Press, Boca Raton, USA.

Demarchi, L., Bizzi, S., Piégay, H., 2016. Hierarchical object-based mapping of riverscape units and in-stream mesohabitats using LiDAR and VHR imagery. Remote Sens. 8, 97. doi:10.3390/rs8020097

Duro, D.C., Franklin, S.E., Dubé, M.G., 2012. A comparison of pixel-based and object-based image analysis with selected machine learning algorithms for the classification of agricultural landscapes using SPOT-5 HRG imagery. Remote Sens. Environ. 118, 259–272. doi:10.1016/j.rse.2011.11.020

Eisavi, V., Homayouni, S., Yazdi, A.M., Alimohammadi, A., 2015. Land cover mapping based on random forest classification of multitemporal spectral and thermal images. Environ. Monit. Assess. 187, 291. doi:10.1007/s10661-015-4489-3

Favalli, M., Karátson, D., Mazzarini, F., Pareschi, M.T., Boschi, E., 2009. Morphometry of scoria cones located on a volcano flank: A case study from Mt. Etna (Italy), based on high-resolution LiDAR data. J. Volcanol. Geotherm. Res. 186, 320–330. doi:10.1016/j.jvolgeores.2009.07.011

Genuer, R., Poggi, J.-M., Tuleau-Malot, C., 2010. Variable selection using random forests. Pattern Recognit. Lett. 31, 2225–2236. doi:10.1016/j.patrec.2010.03.014

Gislason, P.O., Benediktsson, J.A., Sveinsson, J.R., 2006. Random Forests for land cover classification. Pattern Recognit. Lett. 27, 294–300. doi:10.1016/j.patrec.2005.08.011

Gregorutti, B., Michel, B., Saint-Pierre, P., 2016. Correlation and variable importance in random forests. Stat. Comput. 1–20. doi:10.1007/s11222-016-9646-1

736 Haralick, R.M., 1979. Statistical and structural approaches to texture. Proc. IEEE 67, 786–804.
737 doi:10.1109/PROC.1979.11328

738 Head, E.M., Maclean, A.L., Carn, S.A., 2013. Mapping lava flows from Nyamuragira volcano (1967–2011)
739 with satellite data and automated classification methods. Geomatics, Nat. Hazards Risk 4, 119–144.
740 doi:10.1080/19475705.2012.680503

741 Kahle, A.B., Gillespie, A.R., Abbott, E.A., Abrams, M.J., Walker, R.E., Hoover, G., Lockwood, J.P., 1988.
742 Relative dating of Hawaiian lava flows using multispectral thermal infrared images: A new tool for
743 geologic mapping of young volcanic terranes. J. Geophys. Res. 93, 15239–15251.
744 doi:10.1029/JB093iB12p15239

745 Kassouk, Z., Thouret, J.-C., Gupta, A., Solikhin, A., Liew, S.C., 2014. Object-oriented classification of a
746 high-spatial resolution SPOT5 image for mapping geology and landforms of active volcanoes:
747 Semeru case study, Indonesia. Geomorphology 221, 18–33. doi:10.1016/j.geomorph.2014.04.022

748 Kauahikaua, J.P., Tilling, R.I., 2014. Natural hazards and risk reduction in Hawai'i, in: Poland, M.P.,
749 Takahashi, T.J., Landowski, C.M. (Eds.), Characteristics of Hawaiian Volcanoes. U.S.Geological
750 Survey, Hawaii, USA, pp. 397–427.

751 Kervyn, M., Kervyn, F., Goossens, R., Rowland, S.K., Ernst, G.G.J., 2007. Mapping volcanic terrain using
752 high-resolution and 3D satellite remote sensing. Geol. Soc. London, Spec. Publ. 283, 5–30.
753 doi:10.1144/SP283.2

754 Kim, M., Madden, M., Warner, T., 2008. Estimation of optimal image object size for the segmentation of
755 forest stands with multispectral IKONOS imagery, in: Blaschke, T., Lang, S., Hay, G.J. (Eds.), Object-
756 Based Image Analysis. Springer Berlin Heidelberg, Heidelberg, Germany, pp. 291–307.
757 doi:10.1007/978-3-540-77058-9_16

758 Kitagawa, S., Fukui, K., Takagi, A., 2007. The December 1996 eruption at Nyamuragira, Africa, viewed
759 from JERS-1 InSAR, in: Progress of Crustal and Deformation Research by Space Geodesy and
760 Remote-Sensing Techniques. Kyoto University, Kyoto, pp. 1–33.

761 Legeley-Padovani, A., Mering, C., Guillande, R., Huaman, D., 1997. Mapping of lava flows through SPOT
762 images an example of the Sabancaya volcano (Peru). Int. J. Remote Sens. 18, 3111–3133.
763 doi:10.1080/014311697217008

764 Li, L., Canters, F., Solana, C., Ma, W., Chen, L., Kervyn, M., 2015a. Discriminating lava flows of different
765 age within Nyamuragira's volcanic field using spectral mixture analysis. Int. J. Appl. Earth Obs.
766 Geoinf. 40, 1–10. doi:10.1016/j.jag.2015.03.015

767 Li, L., Solana, C., Canters, F., Chan, J., Kervyn, M., 2015b. Impact of environmental factors on the spectral
768 characteristics of lava surfaces: Feld spectrometry of basaltic lava flows on Tenerife, Canary Islands,
769 Spain. Remote Sens. 7, 16986–17012. doi:10.3390/rs71215864

770 Li, X., Shao, G., 2014. Object-based land-cover mapping with high resolution aerial photography at a
771 county scale in Midwestern USA. Remote Sens. 6, 11372–11390. doi:10.3390/rs61111372

772 Liaw, A., Wiener, M., 2002. Classification and Regression by randomForest. R News 2, 18–22.

773 Liu, D., Xia, F., 2010. Assessing object-based classification: Advantages and limitations. Remote Sens. Lett.
774 1, 187–194. doi:10.1080/01431161003743173

775 Lu, Z., Rykhus, R., Masterlark, T., Dean, K.G., 2004. Mapping recent lava flows at Westdahl Volcano,
776 Alaska, using radar and optical satellite imagery. Remote Sens. Environ. 91, 345–353.
777 doi:10.1016/j.rse.2004.03.015

778 Ma, W., Gong, C., Hu, Y., Li, L., Meng, P., 2015. A multi-characteristic based algorithm for classifying
779 vegetation in a plateau area: Qinghai Lake watershed, northwestern China, in: Shen, C., Yang, W.,
780 Liu, H. (Eds.), Proc. SPIE 9675, AOPC 2015: Image Processing and Analysis. p. 96750L.
781 doi:10.1117/12.2197777

782 Mahmood, A., Giugni, L.P., 2001. Mapping recent lava flows with Radarsat-1 imagery, in: 2001 IEEE
783 International Geoscience and Remote Sensing Symposium. IEEE, Sydney, Australia, pp. 482–484.
784 doi:10.1109/IGARSS.2001.976197

785 Mazzarini, F., Pareschi, M.T., Favalli, M., Isola, I., Tarquini, S., Boschi, E., 2007. Lava flow identification
786 and aging by means of lidar intensity: Mount Etna case. J. Geophys. Res. 112, B02201.
787 doi:10.1029/2005JB004166

788 Murcia, H., Németh, K., Moufti, M.R., Lindsay, J.M., El-Masry, N., Cronin, S.J., Qaddah, A., Smith, I.E.M.,
789 2014. Late Holocene lava flow morphotypes of northern Harrat Rahat, Kingdom of Saudi Arabia:
790 Implications for the description of continental lava fields. J. Asian Earth Sci. 84, 131–145.
791 doi:10.1016/j.jseaes.2013.10.002

792 Myint, S.W., Gober, P., Brazel, A., Grossman-Clarke, S., Weng, Q., 2011. Per-pixel vs. object-based
793 classification of urban land cover extraction using high spatial resolution imagery. Remote Sens.
794 Environ. 115, 1145–1161. doi:10.1016/j.rse.2010.12.017

795 Ouyang, Z.-T., Zhang, M.-Q., Xie, X., Shen, Q., Guo, H.-Q., Zhao, B., 2011. A comparison of pixel-based
796 and object-oriented approaches to VHR imagery for mapping saltmarsh plants. Ecol. Inform. 6,
797 136–146. doi:10.1016/j.ecoinf.2011.01.002

798 Riggan, N.D., Weih, R.C., 2009. A comparison of pixel-based versus object-based land use/land cover
799 classification methodologies. J. Ark. Acad. Sci. 63, 145–152.

800 Rowland, S.K., 1996. Slopes, lava flow volumes, and vent distributions on Volcán Fernandina, Galápagos
801 Islands. J. Geophys. Res. Solid Earth 101, 27657–27672. doi:10.1029/96JB02649

802 Servadio, Z., Villeneuve, N., Bachlery, P., 2012. Automatic mapping of the lava flows at piton de la
803 Fournaise volcano, by combining thermal data in near and visible infrared, in: Escalante, B. (Ed.),
804 Remote Sensing - Applications. InTech, Rijeka, Croatia, pp. 201–220. doi:10.5772/37685

805 Smets, B., Kervyn, M., D'Oreye, N., Kervyn, F., 2015. Spatio-temporal dynamics of eruptions in a youthful
806 extensional setting: Insights from Nyamulagira Volcano (D.R. Congo), in the western branch of the
807 East African Rift. Earth-Science Rev. 150, 305–328. doi:10.1016/j.earscirev.2015.08.008

808 Smets, B., Wauthier, C., D'Oreye, N., 2010. A new map of the lava flow field of Nyamulagira (D.R. Congo)
809 from satellite imagery. J. African Earth Sci. 58, 778–786.

810 Smith, A., 2010. Image segmentation scale parameter optimization and land cover classification using
811 the Random Forest algorithm. J. Spat. Sci. 55, 69–79. doi:10.1080/14498596.2010.487851

812 Smithsonian Institution, 2013. Global Volcanism Program: Fernandina [WWW Document]. Volcanoes of
813 the World.

814 Strobl, C., Boulesteix, A.-L., Kneib, T., Augustin, T., 2008. Conditional variable importance for random
815 forests. BMC Bioinformatics 9, 307. doi:10.1186/1471-2105-9-307

816 Tarquini, S., Favalli, M., 2010. A microscopic information system (MIS) for petrographic analysis. Comput.
817 Geosci. 36, 665–674. doi:10.1016/j.cageo.2009.09.017

818 Thonnard, R.L.G., Denaeyer, N.E., 1965. Carte volcanologique des Virunga (Afrique centrale),
819 introduction générale et notice explicative de la feuille No. 1.

820 Thouret, J.-C., Kassouk, Z., Gupta, A., Liew, S.C., Solikhin, A., 2015. Tracing the evolution of 2010 Merapi
821 volcanic deposits (Indonesia) based on object-oriented classification and analysis of multi-temporal,
822 very high resolution images. Remote Sens. Environ. 170, 350–371. doi:10.1016/j.rse.2015.09.028

823 Tolosi, L., Lengauer, T., 2011. Classification with correlated features: unreliability of feature ranking and
824 solutions. Bioinformatics 27, 1986–94. doi:10.1093/bioinformatics/btr300

825 Trimble, 2011. eCognition Developer 8.7 Referrence Book. Munich, Germany.

826 Vaglio Laurin, G., Chan, J.C.-W., Chen, Q., Lindsell, J.A., Coomes, D.A., Guerriero, L., Frate, F. Del,
827 Miglietta, F., Valentini, R., 2014. Biodiversity mapping in a tropical West African forest with
828 airborne hyperspectral data. PLoS One 9, e97910. doi:10.1371/journal.pone.0097910

829 Weih, R.C., Riggan, N.D., 2010. Object-based classification vs. pixel-based classification: comparative
830 importance of multi-resolution imagery, in: International Archives of the Photogrammetry, Remote
831 Sensing and Spatial Information Sciences. Ghent, Belgium, pp. 1–6.

832 Whiteside, T.G., Boggs, G.S., Maier, S.W., 2011. Comparing object-based and pixel-based classifications
833 for mapping savannas. Int. J. Appl. Earth Obs. Geoinf. 13, 884–893. doi:10.1016/j.jag.2011.06.008

834 Zebker, H.A., Rosen, P., Hensley, S., Mouginis-Mark, P.J., 1996. Analysis of active lava flows on Kilauea
835 volcano, Hawaii, using SIR-C radar correlation measurements. Geology 24, 495–498.
836 doi:10.1130/0091-7613(1996)024<0495:AOALFO>2.3.CO;2

837